

Supporting Information

Construction of self-supporting Ni₂P-WO₃ heterostructure for highly efficient hydrogen evolution under both caustic and acidic conditions

Benzhi Wang,^{a,1} Lixia Wang,^{a,1} Yongteng Qian,^c Yuting Yang,^a Tayirjan Taylor Isimjan,^{b,*} Xiulin Yang^{a,}

*

^a *Guangxi Key Laboratory of Low Carbon Energy Materials, School of Chemistry and Pharmaceutical Sciences, Guangxi Normal University, Guilin 541004, China*

^b *Saudi Arabia Basic Industries Corporation (SABIC) at King Abdullah University of Science and Technology (KAUST), Thuwal 23955-6900, Saudi Arabia*

^c *Department of Physics and Interdisciplinary Course of Physics and Chemistry, Sungkyunkwan University, 2066, Seobu-ro, Jangan-gu, Suwon, Gyeonggi-do 16419, Republic of Korea*

¹ *These authors contributed equally.*

E-mail: xlyang@gxnu.edu.cn; isimjant@sabic.com

Materials

Nickel nitrate hexahydrate ($\text{Ni}(\text{NO}_3)_2 \cdot 6\text{H}_2\text{O}$, ≥98%), nickel chloride hexahydrate ($\text{NiCl}_2 \cdot 6\text{H}_2\text{O}$, ≥98%), ammonium tungstate hydrate ($(\text{NH}_4)_{10}\text{H}_2(\text{W}_2\text{O}_7)_6 \cdot x\text{H}_2\text{O}$), and sodium hypophosphite monohydrate ($\text{NaH}_2\text{PO}_2 \cdot \text{H}_2\text{O}$, 99%). All reagents were purchased from Aladdin and were analytical reagents and used without further purification. Commercial Pt/C (20 wt% for platinum) was purchased from Alfa Aesar. Carbon cloth (CC, WOS1009) was purchased from Taiwan CeTech.

Characterizations

SEM and transmission electron microscopy (TEM, JEOL, JEM-2100F) were conducted to investigate the morphologies and microstructures of the designed catalysts. XRD analysis was conducted to investigate the crystal structures. The chemical states of the samples were examined by XPS. Raman spectroscopy was performed using a confocal Raman microscope (inVia Renishaw, England).

Calculation of active site density and TOF

To determine the TOF values, the number of active sites (n) on the $\text{Ni}_2\text{P}-\text{WO}_x$ catalysts first need to be estimated. This is determined by assuming that both Ni and W species serve as active sites for catalysis, and the total amount of Ni and W (molar content: n) on the surface of the CC is calculated on the basis of the ICP-AES test results (Table S1). The TOF values (s^{-1}) can be calculated using the following equation:¹

$$\text{TOF} = \frac{jA}{2nF}$$

where j is the current density (A cm^{-2}) recorded during the LSV measurement at a certain overpotential, A is the geometric surface area of the catalytic electrode, F is the Faraday constant (C mol^{-1}), and n is the number of active sites (mol) present in the electrode. The 1/2 factor in the equation is due to the fact that two electrons are necessary for the formation of one hydrogen molecule starting from two protons ($2\text{H}^+ + 2e^- \rightarrow \text{H}_2$).

Calculation of electrochemically active surface area (ECSA)

The real surface area of the HER catalyst is calculated from the ECSA, and the ECSA is calculated from the specific capacitance.² The specific capacitance of flat surfaces is typically in the range of 20–60 $\mu\text{F cm}^{-2}_{\text{geo}}$.³

$$A_{\text{ECSA}} = \frac{\text{specific capacitance}}{60 \mu\text{F cm}^{-2}_{\text{geo per cm}} \text{cm}^{-2}_{\text{ECSA}}}$$

From Figure 4d, ECSA can be calculated for $\text{Ni}_2\text{P}-\text{WO}_3/\text{CC}-0$, $\text{Ni}_2\text{P}-\text{WO}_3/\text{CC}-10$, $\text{Ni}_2\text{P}-\text{WO}_3/\text{CC}-30$, $\text{Ni}_2\text{P}-\text{WO}_3/\text{CC}-60$, $\text{Ni}_2\text{P}-\text{WO}_3/\text{CC}-90$ and Pt/C/CC .

$$A_{\text{ECSA}}(\text{Ni}_2\text{P}-\text{WO}_3/\text{CC}-0) = \frac{1.0 \text{ mF cm}^{-2}}{60 \mu\text{F cm}^{-2}_{\text{geo per cm}} \text{cm}^{-2}_{\text{ECSA}}} = 16.7 \text{ cm}^2_{\text{ECSA}}$$

$$A_{\text{ECSA}}(\text{Ni}_2\text{P}-\text{WO}_3/\text{CC}-10) = \frac{7.7 \text{ mF cm}^{-2}}{60 \mu\text{F cm}^{-2}_{\text{geo per cm}} \text{cm}^{-2}_{\text{ECSA}}} = 128.3 \text{ cm}^2_{\text{ECSA}}$$

$$A_{\text{ECSA}}(\text{Ni}_2\text{P}-\text{WO}_3/\text{CC}-30) = \frac{12.7 \text{ mF cm}^{-2}}{60 \mu\text{F cm}^{-2}_{\text{geo per cm}} \text{cm}^{-2}_{\text{ECSA}}} = 211.7 \text{ cm}^2_{\text{ECSA}}$$

$$A_{\text{ECSA}}(\text{Ni}_2\text{P}-\text{WO}_3/\text{CC}-60) = \frac{36.4 \text{ mF cm}^{-2}}{60 \mu\text{F cm}^{-2}_{\text{geo per cm}} \text{cm}^{-2}_{\text{ECSA}}} = 606.7 \text{ cm}^2_{\text{ECSA}}$$

$$A_{\text{ECSA}}(\text{Ni}_2\text{P}-\text{WO}_3/\text{CC}-90) = \frac{25.7 \text{ mF cm}^{-2}}{60 \mu\text{F cm}^{-2}_{\text{geo per cm}} \text{cm}^{-2}_{\text{ECSA}}} = 428.3 \text{ cm}^2_{\text{ECSA}}$$

$$A_{\text{ECSA}}(\text{Pt/C}) = \frac{125.7 \text{ mF cm}^{-2}}{60 \mu\text{F cm}^{-2}_{\text{geo per cm}} \text{cm}^{-2}_{\text{ECSA}}} = 2095.0 \text{ cm}^2_{\text{ECSA}}$$

Calculation of normalized electrochemically active surface area (ECSA)

In order to reflect the intrinsic catalytic activity, we normalized the electrochemically active surface area of the catalytic activity.

$$J_{\text{ECSA}} = \frac{J \text{ mA}}{A_{\text{ECSA}}}$$

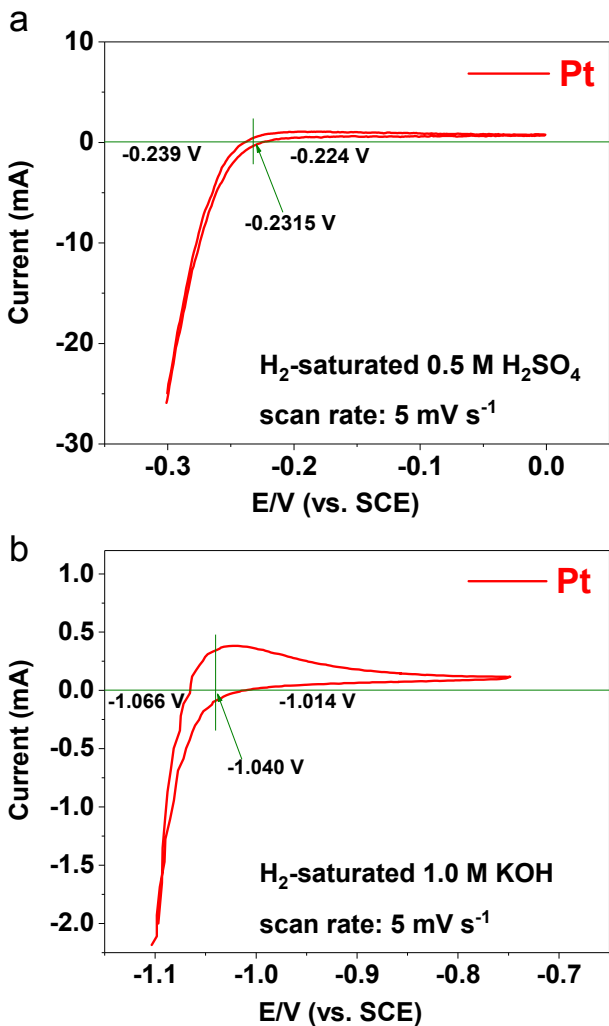


Fig. S1. RHE voltage calibration. The calibration was performed in the high purity hydrogen saturated electrolyte with a Pt wire as the working electrode. Current–voltage scans were run at a scan rate of 5 mV s^{-1} , and the average of the two potentials at which the current crossed zero was taken to be the thermodynamic potential for the hydrogen electrode reactions. Our result shows that the E(SCE) is lower than E(RHE) by 0.232 V and 1.040 V in $0.5 \text{ M H}_2\text{SO}_4$ and 1.0 M KOH , respectively. This value is consistent with the values of 0.250 V and 1.040 V estimated from the Nernst equation. The pH value is 0.15 for the $0.5 \text{ M H}_2\text{SO}_4$ solution, which yields a value of $E(\text{RHE}) = E(\text{SCE}) + 0.241 + 0.059 \text{ pH} = E(\text{SCE}) + 0.250$. The pH value of 13.54 for 1.0 M KOH solution and the $E(\text{RHE}) = E(\text{SCE}) + 0.241 + 0.059 \text{ pH} = E(\text{SCE}) + 1.040$.

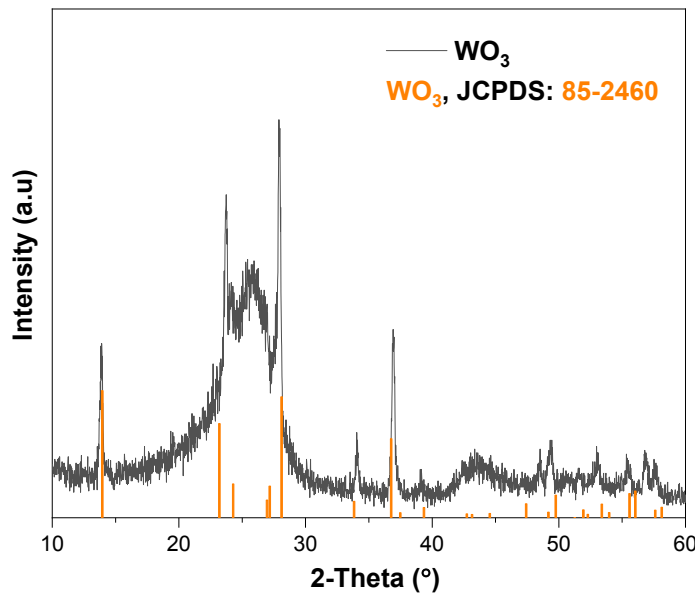


Fig. S2. XRD patterns of WO_3 .

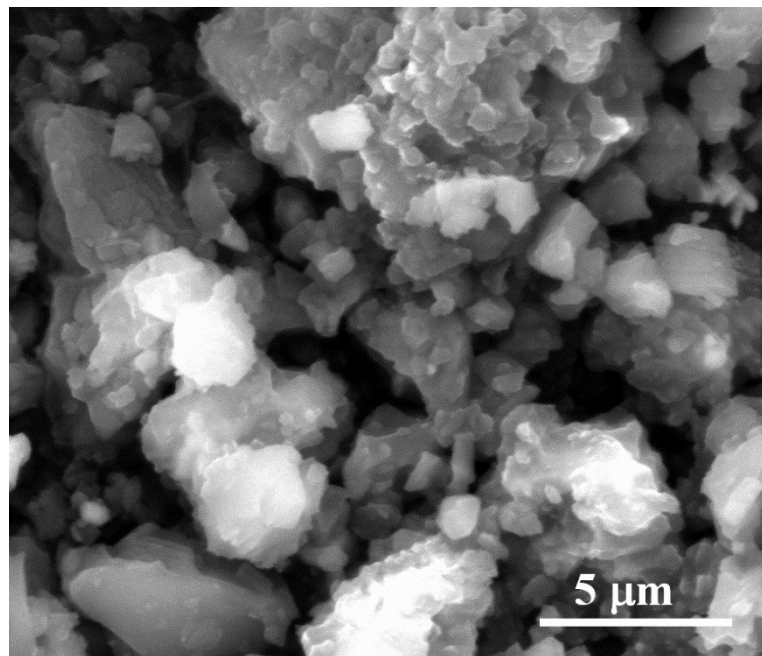


Fig. S3. SEM image of the synthesized Ni_2P powder.

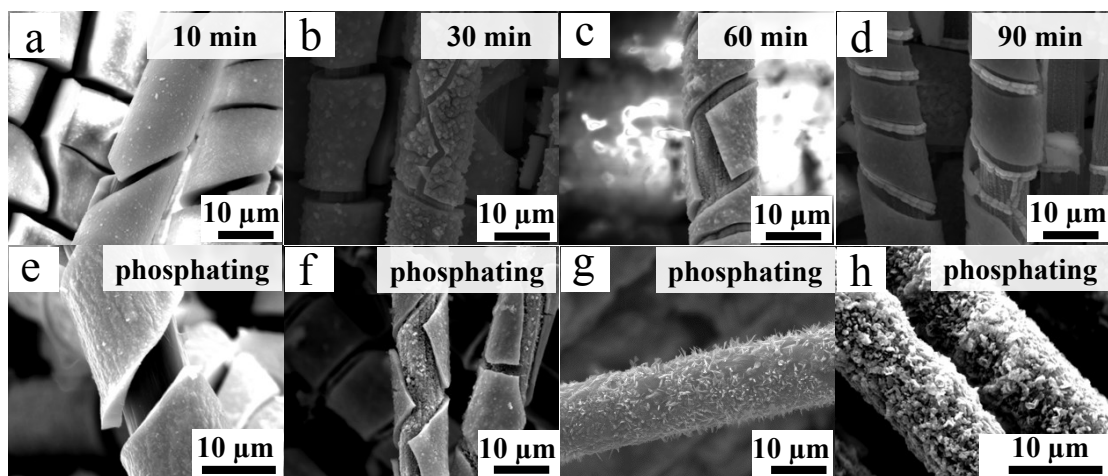


Fig. S4. SEM images of electrodeposited tungsten with different electrodeposition times before and after phosphidation.

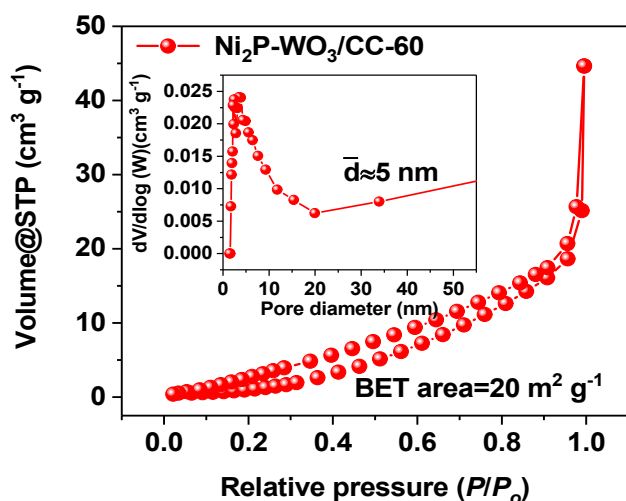


Fig. S5. Nitrogen adsorption-desorption isotherms of $\text{Ni}_2\text{P}-\text{WO}_3$ -60.

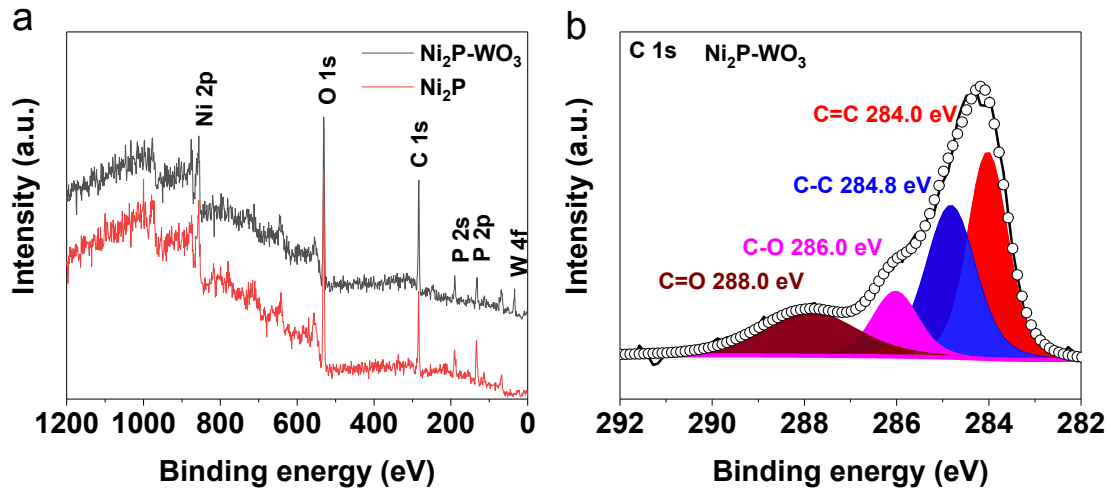


Fig. S6. XPS full-range survey spectra of (a) $\text{Ni}_2\text{P}-\text{WO}_3$ and Ni_2P and (b) the C 1s spectrum of $\text{Ni}_2\text{P}-\text{WO}_3$.

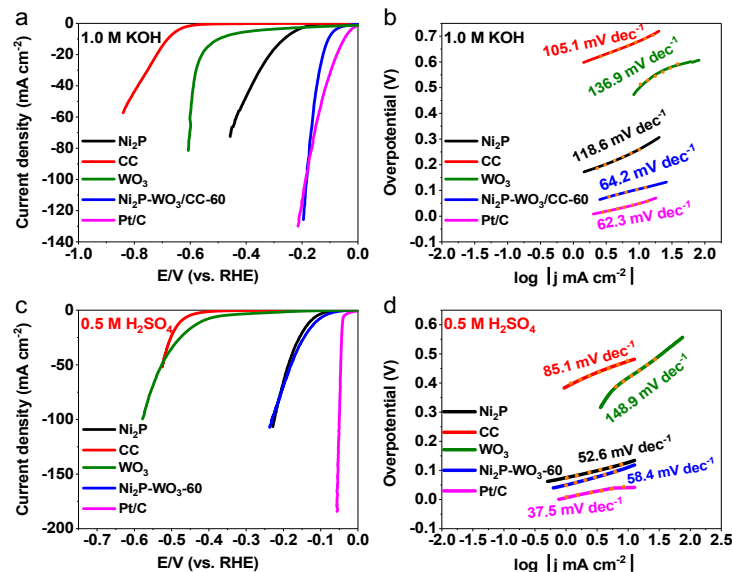


Fig. S7. (a) and (c) LSV polarization curves and (b) and (d) corresponding Tafel slopes of Ni_2P , CC, WO_3 -P, $\text{Ni}_2\text{P}-\text{WO}_3$ -60, and 20 wt.% Pt/C in 1.0 M KOH and 0.5 M H_2SO_4 .

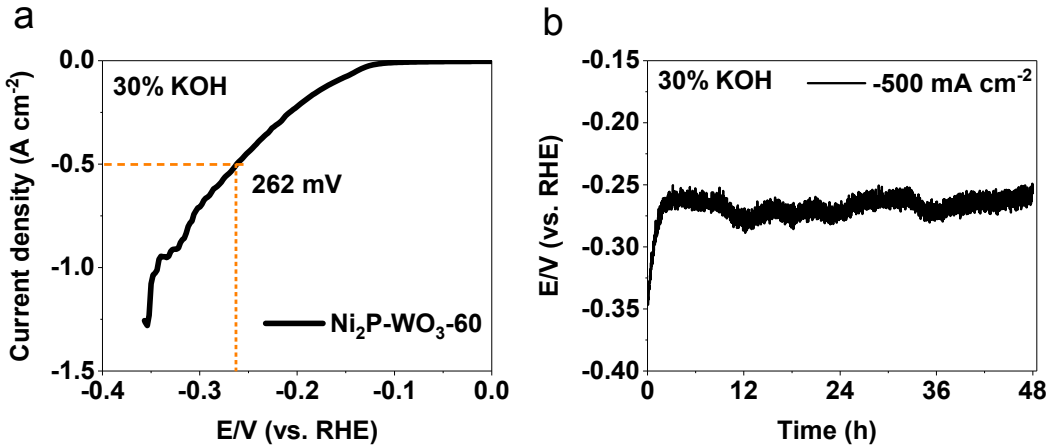


Fig. S8. (a) LSV polarization curves and (b) durability tests of $\text{Ni}_2\text{P}-\text{WO}_3$ -60 at -500 mA cm^{-2} in 30% KOH solution.

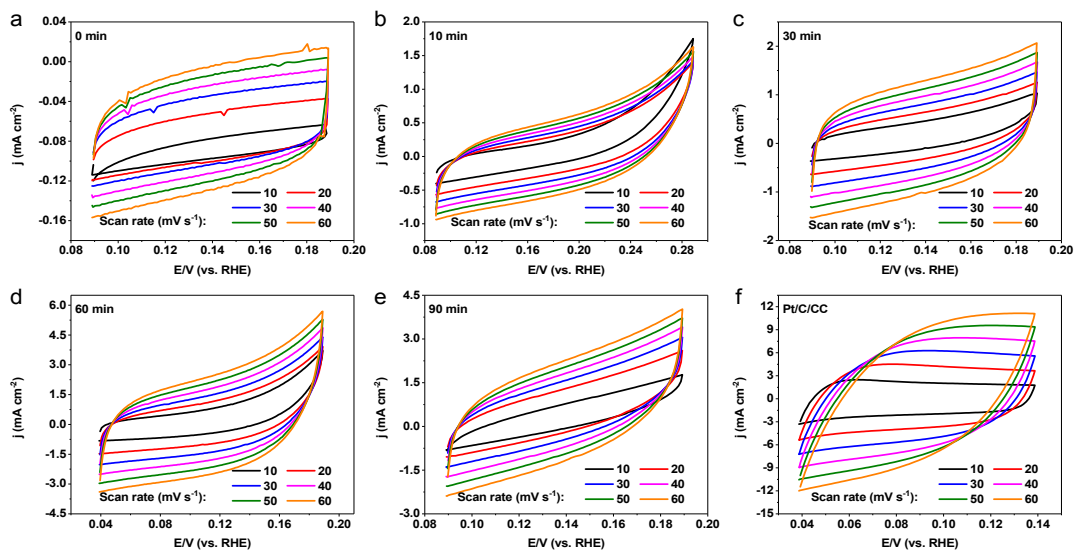


Fig. S9. Cyclic voltammograms with different scan rates of $\text{Ni}_2\text{P}-\text{WO}_3$ and Pt/C/CC catalysts tested in non-faradaic potential windows in 1.0 M KOH.

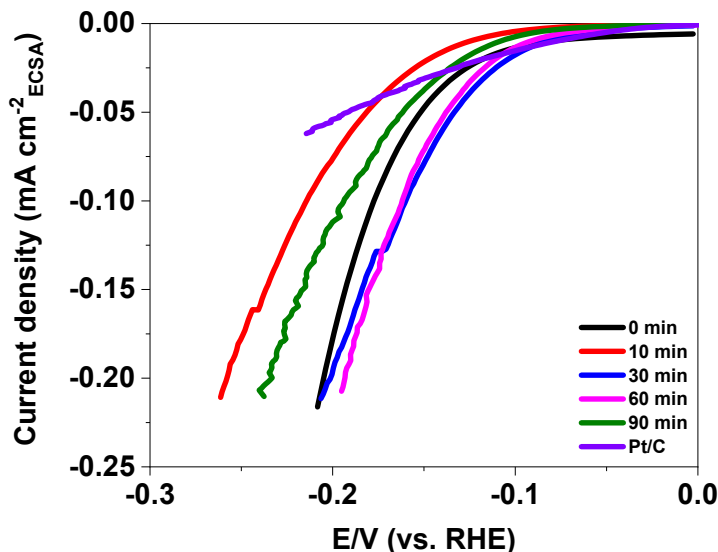


Fig. S10. Polarization curves of $\text{Ni}_2\text{P}-\text{WO}_3$ and Pt/C catalysts normalized by the ECSA.

Tables:

Table S1. Inductive coupled plasma atomic emission spectroscopy (ICP-AES) results of the mass fraction of W and Ni in composite materials after electrodepositing W for different times.

W electrodeposition time	Ni (%)	W (%)	Molar ratio of Ni/W
10 min	66.93	4.3	42.49/1
30 min	47.84	20.05	7.46/1
60 min	38.45	17.11	7.04/1
90 min	39.3	16.86	7.31/1

Note: In this work, the mass of CC was determined prior to electrodeposition, and then the mass of the composite materials was determined after electrodeposition by difference. The catalyst was then dissolved in 12 mL of aqua regia, and 15 μL of the solution was removed with a pipette and diluted with water in 100 mL volumetric flask. Finally, the concentrations of Ni and W were measured by ICP-AES.

Table S2. Summary of previously reported transition-metal HER catalysts in alkaline solutions.

Catalyst	η_{10} (mV)	Tafel slope (mV dec ⁻¹)	References
Ni₂P-WO₃/CC	105	64.2	This work
Ni-Cu-P	120	69.0	ACS Appl. Mater. Interfaces 2018, 10, 41,35224-35233
mC-Mo-850	145	55	Adv. Funct. Mater. 2019, 29, 1807419
Cu plate@CMO	252	N/A	Appl. Catal. B: Environ. 2019, 249, 227-234
Ni-Mo-P	~150	76.4	Nanoscale, 2019, 11, 9353-9361
MoS ₂ /LDH	110	77	Nano Lett. 2019, 19, 7, 4518-4526
Co@N-	108	55	Adv. Mater. 2018, 30, 1802011
CNTs@rGO			
Cu–Ni nanocages	140	79	ACS Catal. 2019, 9, 5084-5095
Cu–TiO _x –Ti	108	122	ACS Appl. Mater. Interfaces 2018, 10, 35, 29583-29592
iCoN/C nanocages	103	N/A	Adv. Mater. 2019, 31, 1805541
Ni/V ₂ O ₃	140	112	Chem. Commun., 2019, 55, 3290-3293
Ni ₂ P@NiFeAlO _x	105	106	Inorg. Chem. 2019, 58, 5, 3247-3255

Table S3. Summary of previously reported transition-metal HER catalysts in acid solutions.

Catalyst	η_{10} (mV)	Tafel slope (mV dec ⁻¹)	References
Ni₂P-WO₃/CC	107	55.9	This work
Ni-Cu-P	150	N/A	ACS Appl. Mater. Interfaces 2018, 10, 41, 35224-35233
N-MoS ₂ /CN	114	46.8	J. Am. Chem. Soc. 2019, 141, 18578-18584
Mo _x C-0.4	155	48	Appl. Catal. B: Environ. 2019, 247, 78-85
MoS _x	180	~50	ACS Catal. 2019, 9, 2368-2380
Cu plate@CMO	~250	N/A	Appl. Catal. B: Environ. 2019, 249, 227-234
NP-MoS ₂	116	58.4	Nano Energy 2019, 58, 862-869
Ni ₂ P@PCG	110	58.6	J. Mater. Chem. A, 2018, 6, 24107-24113
NiMo ₆ O ₂₄ @Cu/TNA	~220	89.2	Appl. Catal. B: Environ. 2019, 249, 163-171

L-Mo ₂ C	170	77	ACS Appl. Mater. Interfaces 2018, 10, 47, 40500-40508
11N-Ti ₂ CT _x	215	67	J. Mater. Chem. A , 2018, 6 , 20869-20877
Ni-CoP/HPPFs	144	52	Nano Energy 2019, 56, 411-419

Table S4. Comparison of the overall-water-splitting activities among different earth-abundant electrocatalysts tested in 1.0 M KOH.

Catalyst (Cathode)	Catalyst (Anode)	E (V) @ <i>j</i> (mA cm ⁻²)	References
Ni₂P-WO₃/CC-60	RuO₂	1.58@10 1.73@100	This work
CoP-Co ₂ P@PC/PG	CoP-Co ₂ P@PC/PG	1.57@10 ~1.81@100	Small 2019, 1804546
(Ni, Fe)S ₂ @MoS ₂	(Ni, Fe)S ₂ @MoS ₂	1.56@10 1.72@100	Appl. Catal. B: Environ. 2019, 247,107-114
N-NiMoO ₄ /NiS ₂	N-NiMoO ₄ /NiS ₂	1.60@10 1.98@100	Adv. Funct. Mater. 2019, 29,1805298
Ni ₃ (S _{0.25} Se _{0.75}) ₂ @ NiOOH-8	Ni ₃ (S _{0.25} Se _{0.75}) ₂ @ NiOOH- 8	1.55@10 1.90@100	Small 2018, 1803666
Ni ₃ S ₂ @MoS ₂ /FeOOH	Ni ₃ S ₂ @MoS ₂ /FeOOH	1.57@10 ~1.75@100	Appl. Catal. B: Environ. 2019, 244, 1004- 1012
LiCoBPO/NF	LiCoBPO/NF	1.53@10 1.73@100	Energy Environ. Sci. 2019,12, 988-999
Ni ₃ FeN/r-GO-20	Ni ₃ FeN/r-GO-20	1.60@10 ~1.95@100	ACS Nano 2018,12,245-253
Fe-Ni@NC-CNTS	Fe-Ni@NC-CNTS	~1.86@50 ~1.92@100	Angew. Chem. Int. Ed. 2018, 57, 8921-8926
CoP NPs@NF	CoP NPs@NF	1.71@50 1.78@100	Nano Energy 2018, 53, 286-295

References

- 1 P. Karfa, K. C. Majhi and R. Madhuri, *ACS Catal.*, 2018, **8**, 8830-8843.
- 2 Y. Zhu, H. A. Tahini, Z. Hu, J. Dai, Y. Chen, H. Sun, W. Zhou, M. Liu, S. C. Smith, H. Wang and Z. Shao, *Nat. Commun.*, 2019, **10**, 149.
- 3 Q. Wu, M. Luo, J. Han, W. Peng, Y. Zhao, D. Chen, M. Peng, J. Liu, F. M. F. de Groot and Y. Tan, *ACS Energy Lett.*, 2020, **5**, 192-199.